Carbohydrate Polymers 101 (2014) 1255–1264

Contents lists available at ScienceDirect

Carbohydrate Polymers

journal homepage: www.elsevier.com/locate/carbpol

Gum ghatti and Fe_3O_4 magnetic nanoparticles based nanocomposites for the effective adsorption of rhodamine B

H. Mittal, Shivani B. Mishra*

Department of Applied Chemistry, University of Johannesburg, South Africa

ARTICLE INFO

Article history:
Received 9 July 2013
Received in revised form 4 September 2013
Accepted 14 September 2013
Available online 22 September 2013

Keywords:
Rhodamine B
Adsorption
Gum ghatti
Nanocomposite
Isotherms
Thermodynamics

ABSTRACT

This article reports the development of a new nanocomposite using gum ghatti crosslinked with poly(acrylic acid-co-acrylamide) reinforced with iron oxide magnetic nanoparticles. The nanocomposite was characterized through BET, FT-IR, XRD, SEM-EDX, TGA and TEM and applied for the removal of RhB. Different optimized adsorption parameters were adsorbent dose (0.8 g/L) and pH (7.0). The adsorption isotherm data was used to study Langmuir, Freundlich and Dubinin–Kaganer–Radushkevich isotherm models. The value of correlation coefficient confirmed the applicability of Langmuir isotherm model with maximum adsorption efficiency of 654.87 mg/g. The adsorption kinetics data showed pseudo second order reaction. Thermodynamic studies showed that the adsorption process was endothermic and spontaneous. Moreover, the adsorbent was successfully utilized for successive three cycles for the adsorption–desorption of RhB.

1. Introduction

Water is one of the most essential natural resources for human life and only 0.03% of the total water available on earth can be utilized for various human activities. Increasing population growth and industrial booms have increased the demand of water, whereas the total availability of the water has remained constant. Moreover, poor water management at industrial level has also reduced the amount of available water. The waste water from textile industries contains a wide variety of toxic dyes which affect human health as well as photosynthetic process in aquatic biota (Goncalves, Ferra, & Amorim, 1996). Because of the high solubility of dyes in water, these are practically non-degradable and further these cannot be degraded in the sludge treatment plants (Kumari & Abraham, 2007). A lot of methods like coagulation/flocculation, photocatalysis, chemical oxidation and microbiological or enzymatic degradation (Allegre, Maisseu, Charbit, & Moulina, 2004; Hao, Kim, & Chiang, 2000) have been previously used for the treatment of dye contaminated water but they are generally ineffective for the complete removal of dyes. Adsorption of different pollutants including dyes on some solid material is the method of choice for the treatment of waste water (Crini, 2006; Papic, Koprivanac, Bozic, & Metes, 2004). Biopolymers based adsorbents is one of the most promising class of adsorbents that have been used for the decontamination of waste water. In recent years numerous biopolymers based adsorbents such as poly(methacrylic acid) grafted functionalized guar gum (Singh, Kumari, Pandey, & Narayan, 2009), cassia grandis seed gum-graft-poly(methylmethacrylate) (Singh, Tiwari, Sharma, & Sanghi, 2007) and 2-acrylamidoglycolic acid grafted xanthan gum (Sand, Yadav, & Behari, 2010) were utilized for the removal of different pollutants from the waste water. Besides a lot of advantages biopolymers suffer some serious drawbacks like poor mechanical strength, water solubility and lack of reusability but it is possible to overcome these drawbacks and control the stability and solubility by the introduction of nanoparticles within the polymer matrix.

Magnetic nanoparticles based adsorbents have attracted significant attention because of their basic properties like very small size, high surface area to volume ratio and easy separation by the application of an external magnetic field (Zhou, Nie, Branford-White, He, & Zhu, 2009). Moreover, they produce no contaminants and because of the magnetic separation they can treat large amount of polluted water within a very short period of time. Different techniques have been developed for the magnetic separation of pollutants from the waste water. Main emphasis on these techniques were given on the fabrication of the natural polymers based adsorbents in which magnetic nanoparticles were incorporated within polymer matrix like gum arabic (Banerjee & Chen, 2007), carboxymethyl-β-cyclodextrin (Badruddoza, Tay, Tan, Hidajat, & Uddin, 2011), chitosan (Chang & Chen, 2005) and calcium

* Corresponding author at: Department of Applied Chemistry, University of Johannesburg, P.O. Box 17011, Doornfontein 2028, South Africa. Tel.: +27 724559377; fax: +27 115596425.
E-mail address: smishra@uj.ac.za (S.B. Mishra).

0144-8617/$ – see front matter © 2013 Elsevier Ltd. All rights reserved.
http://dx.doi.org/10.1016/j.carbpol.2013.09.045

alginate (Lim, Zheng, Zou, & Chen, 2009). Incorporation of magnetic nanoparticles within the polymer matrix not only increases the surface area but also provides additional functionalities for the binding of dye molecules (Xu et al., 2012). Biopolymers based magnetic nanocomposites have been successfully utilized previously for the decontamination of the organic dyes and metallic pollutants from waste water (Banerjee & Chen, 2007; Rocher, Siaugue, Cabuil, & Bee, 2008).

Gum ghatti is an anionic natural polysaccharide and gained great interest towards researchers in recent years. The main structure of Gg has alternating 4-O-subsituted and 2-O-subsituted α-D-mannopyranose units and chains of 1 → 6 linked β-D-galactopyranose with side chains of L-arabinofuranose residue. Graft co-polymers Gg have been extensively used as superabsorbents for the recovery of crude oil in the petroleum industries (Kaith, Jindal, Mittal, & Kumar, 2012) and as flocculants for the treatment of waste water (Rani, Sen, Mishra, & Jha, 2012). It has also been proved that the graft co-polymers of poly(acrylic acid) and poly(acrylamide) with different biopolymers are efficient adsorbents for the removal of pollutants such as heavy metal ions and dyes from waste water (Bhattacharyya, Ray, & Mandal, 2013; Ghorai, Sinhamahpatra, Sarkar, Panda, & Pal, 2012). Rhodamine B is a basic dye and is extensively used in biotechnology as a staining fluorescent dye and in cosmetic products. It is generally toxic and water soluble. It causes irritation in terms of eye and skin contact. It showed carcinogenicity in laboratory. The intravenous median lethal (LD_{50}) of rhodamine B is 89.5 mg/kg. Keeping in view the advantages of biopolymers and iron oxide magnetic nanoparticles based nanocomposites, we synthesized crosslinked polymer network of gum ghatti with acrylic acid-co-acrylamide and incorporated iron oxide magnetic nanoparticles within the polymeric matrix. Nanocomposite showed excellent adsorption efficiency (654.87 mg/g) towards the adsorption of rhodamine B from aqueous solution. Incorporation of magnetic nanoparticles within the polymer matrix and origin of high adsorption properties of nanocomposite were explained in details using morphological and structural characterization results. The adsorption kinetics, isotherms and adsorption thermodynamics were also studied. Desorption studies were also performed to check the reusability and regeneration of the adsorbent.

2. Experimental

2.1. Materials and methods

2.1.1. Chemicals

Gum ghatti (Gg), Acrylic acid (AA), acrylamide (AAm), potassium persulphate (KPS), ascorbic acid (ABC), N,N′-methylene-bis-acrylamide (MBA), rhodamine B (RhB) and iron oxide magnetic nanoparticles (Fe_3O_4 MNPs) were purchased from Sigma Aldrich and used without further purification. Deionized water was used for the preparation of solutions. Stock solution of RhB (1000 mg/L) was prepared by dissolving appropriate amount of dye in the 1000 ml of deionized water and the stock solution was further diluted for batch experiments using deionized water.

2.1.2. Synthesis

For the synthesis of Gg-cl-P(AAm-co-AA)/Fe_3O_4 nanocomposites, crosslinked network of poly(AAm-co-AA) with Gg was prepared through free radical graft co-polymerization technique using KPS and ABC redox pair as an initiator and MBA as a crosslinking agent. Prior to grafting, 50 mg Fe_3O_4 MNPs were added in 20 ml deionized water and sonicated for 4 h for the better dispersion of nanoparticles. After the sonication, Gg (1 g) was added in the reaction mixture and stirred vigorously for the complete dissolution of gum in water. At this stage, a mixture of 30 mg KPS and 20 mg ABC was added in the reaction mixture and the temperature was maintained at 60 °C. 50 mg of MBA was added in the reaction mixture followed by the addition of the mixture of AAm (1 g) and AA (2.5 ml) with constant stirring. After 3 h, the reaction was stopped and cooled at room temperature. Homopolymers were removed by successive soxhlet extraction using acetone as solvent. Finally the product was washed with 250 ml of acetone, dried in hot air oven at 40 °C till a constant weight was achieved.

2.1.3. Characterization

The incorporation of Fe_3O_4 MNPs in the crosslinked network of Gg-cl-P(AAm-co-AA) was confirmed through different techniques like BET, FT-IR, SEM, TEM and XRD. X-ray diffraction study of the samples were done by using Rigaku Ultima IV, X-ray diffractometer employing Cu Kα radiation of the wavelength of 1.5406 Å with visible slights at 45 kV/40 mA. The structural determination and the confirmation of grafting of poly(AA-co-AAm) onto Gg and incorporation of Fe_3O_4 MNPs within the polymer matrix was done through FT-IR (Perkin-Elmer Spectrum 100 spectrometer) using KBR pallet method in the spectral range of 4000–400 cm^{-1} with a resolution of 4 cm^{-1}. The changes in the morphology of Gg after grafting and the polymer matrix after the incorporation of Fe_3O_4 MNPs were studied using scanning electron microscope (TESCAN, VEGA SEM) under a 20 kV electron acceleration voltage coupled with energy dispersive (EDX) for elemental analysis. As the samples were non-conducting in nature so these were coated with carbon for conductive metal coating and the scanning was concurred with the position of beam on the specimen for maintaining small size over a large distance relative to the specimen. Successful incorporation and variation in the size of Fe_3O_4 MNPs within polymer matrix was examined through JEOL JEM-2100F, field emission electron microscope with an accelerating voltage of 90 kV. Small pinch of sample was added in few millilitres of ethanol and sonicated for 30 min. Two drops of sonicated suspension was transferred to the TEM grid and allowed to dry in ambient air. Changes in the thermal properties of polymer matrix after the incorporation of Fe_3O_4 MNPs were studied by using thermogravimetric analysis (Perkin-Elmer TGA 4000, thermogravimetric analyzer). 10 mg of the sample was taken in a platinum crucible and heated with the heating rate of 10 °C min^{-1} in the temperature range of 30–700 °C using oxygen gas. The increase in the BET surface area and porosity of the polymer matrix after the incorporation of Fe_3O_4 MNPs was studied by nitrogen adsorption–desorption measurements using Micromeritics, ASAP 2020, surface area and porosity analyser.

2.2. Adsorption studies

The batch experiments for the adsorption of RhB solution were done in thermostat water bath at 20 °C and 120 rpm for 24 h in 100 ml plastic bottles. Optimization of solution pH and polymer dose was done to get optimized adsorption conditions. Effect of pH on the adsorption of dye was studied over the pH range of 2–11 and the pH was adjusted by using 0.1 M NaOH and 0.1 M HCl solutions. In the typical batch experiments, 0.6 mg/L of nanocomposites was added in 50 ml dye solutions (50 mg/L) taken in plastic bottles and shacked for 24 h over the thermostatic water bath. After 24 h, the bottles were taken out and the suspensions were filtered. Concentration of the RhB dye remained in the solution was analyzed using UV/VIS spectrophotometer (Shimazdu, UV-2450, UV–vis spectrophotometer) at 554 nm as λ_{max} of RhB. Adsorption efficiency or percentage removal was calculated using the equation (Sadeghi, Azhdari, Arabi, & Moghaddam, 2012):

$$\%\text{Removal} = \frac{C_0 - C_e}{C_0} \times 100 \quad (1)$$

where, C_o is the initial concentration (mg/L) and C_e is the equilibrium concentration (mg/L) of RhB.

After the optimization of pH, effect of polymer dose on the adsorption capacity was studied by varying the amount of adsorbent from 0.2 to 1.4 g/L at pre-optimized pH under the same experimental conditions and the percentage removal was calculated using Eq. (1).

Adsorption isotherm experiments were carried-out at three different temperatures (25, 35 and 45 °C) by adding the optimized amount of adsorbent (0.8 g/L) in 50 ml dye solutions of different concentrations (100–500 mg/L) at pH 7.0. The bottles were placed in the water bath and shaked for 24 h. The equilibrium adsorption (q_e) was calculated using the following equation (Bhaumik, Leswifi, Maity, Srinivasu, & Onyango, 2011):

$$q_e = \frac{C_0 - C_e}{m} \times V \quad (2)$$

where, q_e is the equilibrium adsorption of the dye per unit mass of the adsorbent (mg/g), m is the weight of the adsorbent (g) and V is the volume of the dye taken (L).

Experiments for the kinetic studies were done using a mechanical stirrer with a shaking speed of 120 rpm at 20 °C with three different initial dye concentrations i.e. 50, 75 and 100 mg/L. For kinetic studies, 0.8 g of Gg-cl-P(AA-co-AAm)/Fe_3O_4 nanocomposites was added in 1 L of the dye solution and agitated for a varied contact time interval in the range of 0–240 min. At various time intervals 5 ml of the sample aliquot was collected, filtered and remaining concentration of RhB was determined as earlier. Amount of dye adsorbed at different time intervals was calculated using the following equation:

$$q_t = \frac{C_0 - C_t}{m} \times V \quad (3)$$

where, q_t is the amount of dye adsorbed per unit mass of the adsorbent (mg/g) at time t and C_t is the concentration of dye (mg/L) at time t.

2.3. Desorption and reusability experiments

To study the reproducibility and reusability of Gg-cl-P(AA-co-AAm)/Fe_3O_4 nanocomposite for the adsorption of RhB the desorption experiments were carried-out using 0.1 M HCl. Initially, 40 mg of the nanocomposite was added in the 100 mg/L of RhB dye solution and shacked for 24 h. RhB loaded nanocomposite was washed with water, dried, weighed and recycled using 0.1 M HCl. The regenerated sample was again used for the next cycle of the adsorption of RhB. The adsorption–desorption experiments were done for the successive five cycles.

3. Results and discussion

3.1. Characterization of the nanocomposite

Complete characterization of the nanocomposite, uniform distribution of Fe_3O_4 MNPs in the crosslinked polymer matrix, morphological, structural and thermal properties were studied through different techniques such as FT-IR, TEM, SEM-EDX, XRD, BET and TGA.

3.1.1. X-ray diffraction

Fig. S1, Supporting Information represents the XRD patterns of uncoated Fe_3O_4 MNPs and Gg-cl-P(AA-co-AAm)/Fe_3O_4 nanocomposite. In the XRD pattern of uncoated Fe_3O_4 MNPs diffraction peaks were observed at 30.1°, 35.6°, 43.2°, 53.6° and 62.6° at 2θ scale. Incorporation and uniform distribution of Fe_3O_4 MNPs in Gg-cl-P(AA-co-AAm) polymer matrix was confirmed by the presence of all the XRD peaks mentioned above in the XRD pattern of Gg-cl-P(AA-co-AAm)/Fe_3O_4 nanocomposite with a little bit of reduced intensity and the peaks became slightly wider because of the coating of non-magnetic and amorphous Gg-cl-P(AA-co-AAm) polymeric shell (Sadeghi, Azhdari, Arabi, & Moghaddam, 2012).

3.1.2. Fourier transform infra-red spectroscopy

FT-IR spectra of uncoated Fe_3O_4 MNPs and Gg-cl-P(AA-co-AAm)/Fe_3O_4 nanocomposite are shown in Fig S2, Supporting Information. In the FT-IR spectra of uncoated Fe_3O_4 MNPs the characteristic peak of Fe—O bond is shown at 554.93 cm^{-1}. A similar peak was also observed in the FT-IR spectra of Gg-cl-P(AA-co-AAm)/Fe_3O_4 nanocomposite. FT-IR of Gg-cl-P(AA-co-AAm)/Fe_3O_4 nanocomposite showed some other peaks at 2915.68 cm^{-1} due to —OH stretching of AA, 1697.35 cm^{-1} due to —CO stretching of AA, 1653.97 cm^{-1} due to —CO stretching of amide-I, 1454.22 cm^{-1} due to NH in plane bending of amide-II, 1404.51 cm^{-1} due to —CN stretching of amide-III and 761 cm^{-1} due to —OCN deformation of amide-IV in addition to the characteristic peaks of Gg (Kaith, Jindal, Mittal, & Kumar, 2012).

3.1.3. Scanning electron microscopy

The changes in the morphologies of Gg and Gg-cl-P(AA-co-AAm) because of the graft co-polymerization and incorporation of Fe_3O_4 MNPs are studied through scanning electron microscopy. SEM images of Gg, Gg-cl-P(AA-co-AAm) and Gg-cl-P(AA-co-AAm)/Fe_3O_4 nanocomposite are shown in (Fig. S3, Supporting Information). Gg had a very granular, smooth and homogeneous morphology (Fig. S3a, Supporting Information), whereas this smooth surface became heterogeneous, rough and converted to fibrillar structure after the grafting and crosslinking reactions (Fig. S3b, Supporting Information). Surface morphology of the polymer again changed and better matrix coherence was achieved after the incorporation of Fe_3O_4 MNPs. SEM of Gg-cl-P(AA-co-AAm)/Fe_3O_4 nanocomposite showed more coherent and near co-continuous morphology than the fibrillar surface of Gg-cl-P(AA-co-AAm) (Fig. S3c, Supporting Information). Moreover, the presence of Fe peak in the EDX of nanocomposite showed the successful incorporation and uniform distribution of Fe_3O_4 MNPs in the polymer matrix (Fig. S3d, Supporting Information).

3.1.4. Transmission electron microscopy

Fig. S4, Supporting Information shows the typical TEM images of uncoated Fe_3O_4 MNPs and Gg-cl-P(AA-co-AAm)/Fe_3O_4 nanocomposite. Most of the uncoated Fe_3O_4 MNPs had sizes less than 35 nm which are shown in Fig. S4, Supporting Information. It was also observed that magnetic nanoparticles got incorporated in the crosslinked polymer matrix and the mean diameter of the coated nanoparticle was ca 70 nm which was slightly higher than the mean diameter of uncoated magnetic nanoparticles.

3.1.5. Thermal studies

The changes in the thermal properties of Gg-cl-P(AA-co-AAm) after the incorporation of Fe_3O_4 MNPs in the polymer matrix was studied through TGA analysis. TGA of Gg-cl-P(AA-co-AAm) and Gg-cl-P(AA-co-AAm)/Fe_3O_4 nanocomposite is shown in Fig. S5, Supporting Information. It was observed that the initial and final decompositions of Gg-cl-P(AA-co-AAm) were occurred at 163 °C and 470 °C, respectively, whereas after the incorporations of Fe_3O_4 MNPs these decompositions occurred at relatively higher temperatures i.e. 180 °C and 504 °C, respectively in Gg-cl-P(AA-co-AAm)/Fe_3O_4 nanocomposite. Thermal decomposition pattern of Gg-cl-P(AA-co-AAm) had two decomposition stages. First stage decomposition occurred in the temperature range of 163–359 °C with 42% weight loss and this weight loss may be due to the loss of water molecules and volatile components

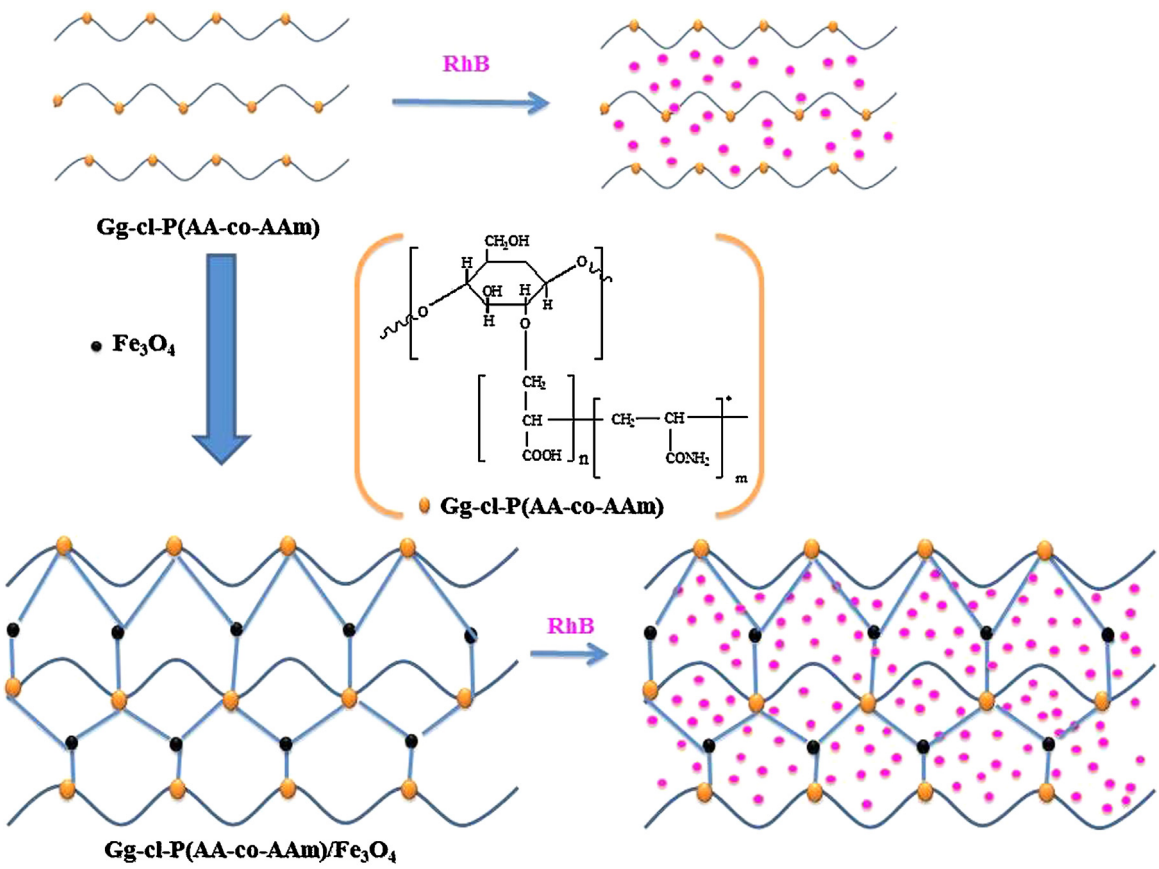

Fig. 1. Proposed mechanism of the RhB adsorption onto Gg-cl-P(AA-co-AAm) and Gg-cl-P(AA-co-AAm)/Fe_3O_4 nanocomposite.

(Mittal, Mishra, Mishra, Kaith, & Jindal, 2013), whereas, second stage decomposition occurred in the temperature range of 359–470 °C with 50.55% weight loss and this weight loss may be due to the breakdown of the polymer matrix and crosslinks between different polymeric chains. However, TGA of Gg-cl-P(AA-co-AAm)/Fe_3O_4 nanocomposite showed two stage decomposition pattern. First stage decomposition was observed in the temperature range of 180–342.5 °C with 23.80% weight loss and the second stage decomposition was observed in the temperature range of 342.5–504 °C with 33% weight loss. In case of Gg-cl-P(AA-co-AAm)/Fe_3O_4 nanocomposite the decompositions occurred at higher temperatures with comparatively lesser weight loss. Therefore, it was observed that the thermal stability of Gg-cl-P(AA-co-AAm) increased after the incorporation of Fe_3O_4 MNPs in the polymer matrix. Moreover, DTG of Gg-cl-P(AA-co-AAm) showed maximum decompositions at 281 °C and 444 °C, whereas, DTG of Gg-cl-P(AA-co-AAm)/Fe_3O_4 nanocomposite showed maximum decompositions at 391.65 °C and 635.4 °C (Fig. S6, Supporting Information). Therefore, TGA and DTG studies clearly showed that the thermal stability of Gg-cl-P(AA-co-AAm) got increased after the incorporation of Fe_3O_4 MNPs in the polymer matrix.

3.1.6. Brunauer–Emmett–Teller (BET) surface area

BET surface area, pore volume and pore diameter of Gg-cl-P(AA-co-AAm) was found to be 0.5965 m^2/g, 0.002845 cm^3/g and 192.3465 Å, respectively and the values of these parameters were increased to 0.9654 m^2/g, 0.005912 cm^3/g and 211.4482 Å, respectively after the incorporation of Fe_3O_4 MNPs in the polymer matrix. Comparison of different BET parameters of Gg-cl-P(AA-co-AAm) and Gg-cl-P(AA-co-AAm)/Fe_3O_4 nanocomposite is shown in Table S1, Supporting Information.

3.2. Adsorption studies

3.2.1. Mechanism of the adsorption

Fig. 1 represents the tentative mechanism for the competitive adsorption of RhB on the surface of Gg-cl(PAA-co-AAm) and Gg-cl(PAA-co-AAm)/Fe_3O_4 nanocomposite. The adsorption capacity of any adsorbent highly depends on its physical and chemical characteristics along with the mass transfer rate (Ghorai, Sinhamahpatra, Sarkar, Panda, & Pal, 2012) and the mass transfer rate depends upon the surface area of the adsorbent. In case of crosslinked graft co-polymer of Gg with P(AA-co-AAm), different polymer chains are closely packed together within a three dimensional polymer framework through covalent bonding between different polymer chains as well as Vander Walls forces of attraction between different non-polar chains and it becomes very difficult for the water molecules to penetrate within the polymer matrix through the closely packed backbone polymer (Gg). Therefore, as a consequence of this the adsorption capacity of the polymer remains low. However, in the presence of Fe_3O_4 MNPs within the polymer matrix, the nanocomposite becomes more flexible and can swell upto much larger extent with an increase in the pore diameter and pore volume. Increased surface area also adds to the increased swelling capacity of the nanocomposite and it shows improved adsorption capacity as compared to the parental polymer matrix. Moreover, presence of nanoparticles in the polymer matrix also increases the functionalities for the binding of dye molecules.

3.2.2. Effect of solution pH on the adsorption of dyes

Solution pH has been found to exert profound effect on the removal of basic dyes by different materials. pH dependent binding process of basic dyes onto different bio-adsorbents have been suggested by a number of researchers (Ncibi, Mahjoub, & Seffen, 2007;

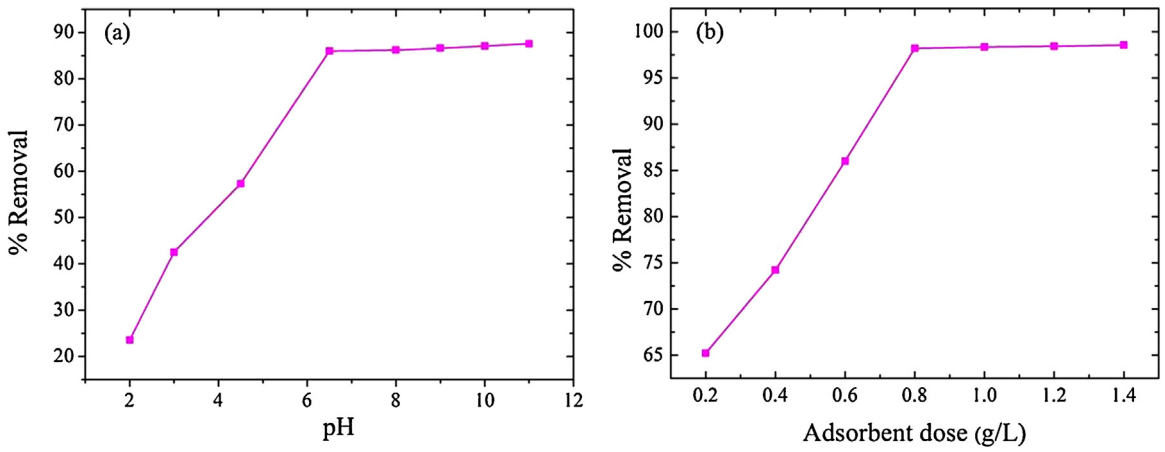

Fig. 2. (a and b): Effect of (a) pH on the adsorption of RhB by Gg-cl-P(AA-co-AAm)/Fe_3O_4 nanocomposite. Conditions: C_o, 50 mg/L; adsorbent dose, 0.6 g/L and temperature, 25 °C and (b) adsorbent dose on the adsorption of RhB by Gg-cl-P(AA-co-AAm)/Fe_3O_4 nanocomposite. Conditions: C_o, 50 mg/L; pH, 7.0 and temperature, 25 °C

Waranusantigul, Pokethitiyook, Kruatrachue, & Upatham, 2003). In the adsorption process of dyes by biosorbents, the role of pH is very important because of its impact on the adsorption sites of the bioadsorbent as well as ionization process of the dye molecules. Effect of pH on the adsorption of RhB onto Gg-cl-P(AA-co-AAm)/Fe_3O_4 nanocomposite was studied in the pH range between 2 and 11 while other adsorption parameters like initial dyes concentration, adsorption dose and shaking time were fixed at 50 mg/L, 0.8 g/L and 24 h, respectively (Fig. 2(a)). Initially, percentage adsorption was found to increase with a change in solution pH from acidic to basic. As shown in figure, percentage adsorption was lowest at pH 2 (23.57%) and increased upto 86% at pH 6.5, then remained almost constant in the pH range of 6–11. Lower adsorption capacity in the acidic medium may be due to the fact that in acidic medium H^+ ions competed effectively with the dyes molecules for the adsorption sites which effectively inhibited the adsorption of dye molecules and ultimately decreased the amount of dye adsorbed. Whereas, in the basic medium the adsorbent got negatively charged and enhanced the adsorption of cationic dyes through electrostatic forces of attraction. Similar results were obtained for the effect of pH for the adsorption of basic dyes on the different adsorbents (Dogan, Alkan, & Onganer, 2000; Khan, Dahiya, & Ali, 2012). The cost and simplicity of the adsorption process are very crucial and important factors for the removal of dye. So, the possibility of the maximum dye removal without the alteration of pH is therefore an advantage and almost constant uptake of dye was observed in the pH range of 6–11, so rest of the studies were performed at pH 7.0.

3.2.3. Effect of polymer dose

A good adsorbent should have the ability to remove relatively higher amount of dye at lower dose along with the lower cost of the adsorption process. Therefore, effect of adsorbent dose on the percentage adsorption of RhB onto Gg-cl-P(AA-co-AAm)/Fe_3O_4 nanocomposite was studied at different polymer dose ranging from 0.2 g/L to 1.4 g/L in neutral medium and is shown in Fig. 2(b). Initially, it was observed that the percentage adsorption increased with increase in polymer dose and about 98% removal was observed with 0.8 g/L adsorbent dose, whereas almost constant adsorption was observed with further increase in amount of adsorbent. Increased adsorption of dye may be due to the increase in the number of adsorption sites with increased adsorbent dose (Bhaumik, Leswifi, Maity, Srinivasu, & Onyango, 2011).

Very high adsorption (>95%) of RhB was achieved using Gg-cl-P(AA-co-AAm)/Fe_3O_4 nanocomposite. This might be because of the reason that the Gg is an anionic polysaccharide (Kaith, Jindal, Mittal, & Kumar, 2012) and have a lot of negatively charged binding sites. Gum polysaccharides based polymers have very good affinity for the binding of cationic impurities. Moreover, the incorporation of Fe_3O_4 MNPs increased the surface area, pore volume as well as the binding sites for the adsorption of cationic impurities within the polymer matrix. RhB is a cationic dye and binds very easily to the anionic adsorbents. Therefore, Gg-cl-P(AA-co-AAm)/Fe_3O_4 nanocomposite adsorbed more than 95% of the RhB from the aqueous solution.

3.2.4. Adsorption isotherm

Adsorption isotherm correlates the amount of dye adsorbed per unit weight of the adsorbent (q_e) with the equilibrium concentration of dye left in the solution (C_e) at different temperatures and indicates the distribution of adsorption molecules between liquid phase and solid phase when the state of equilibrium adsorption reached. Fig. 3(a) shows the isotherm for the adsorption of RhB onto Gg-cl-P(AA-co-AAm)/Fe_3O_4 nanocomposites. An increase in the amount of dye adsorbed was observed with increase in temperature from 25° to 45 °C which showed that the adsorption process in this study was endothermic. Moreover, from Fig. 2(a) it was also observed that in the beginning of the adsorption process, the uptake of RhB molecules at all the temperatures studied increased linearly with the increased initial dye concentration and then attained saturation at higher concentrations. It may be because of the fact that at lower initial lower concentrations, adsorption depends upon the amount of dye transferred from the bulk of the solution to the surface of the adsorbent. On the other hand, at higher initial dye concentration all the adsorption sites get occupied and the adsorption of RhB attains equilibrium (Yan et al., 2012). The experimental isotherm data obtained from the adsorption studies were fitted through the most commonly used Freundlich, Langmuir and Dubinin–Kaganer–Radushkevich (DKR) models (Fig. 3(b–d)).

Freundlich model is usually applicable for the low concentrations and is expressed by the following equation:

$$q_e = K_F \times C_e^{1/n} \quad (4)$$

where, q_e is the equilibrium adsorption concentration of adsorbate per unit mass of the adsorbent (mg/g), C_e is the concentration of adsorbate left in the solution (mg/L), K_F and $1/n$ are the Freundlich constants related to the adsorption capacity and intensity of adsorption. Freundlich constants can be calculated by the logarithmic form of the linearized Eq. (4):

$$\log q_e = \log K_F + \frac{1}{n} \times \log C_e \quad (5)$$

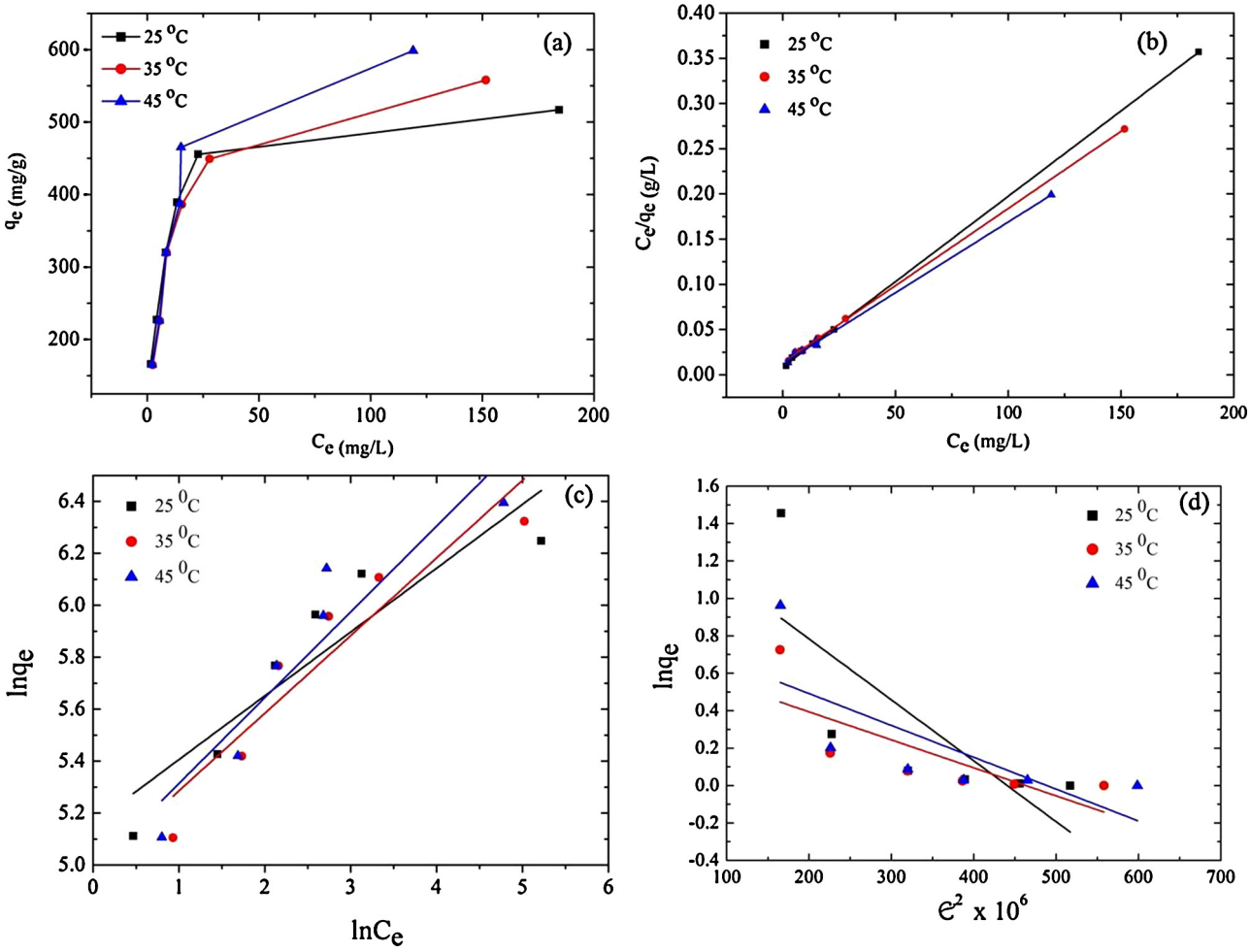

Fig. 3. (a–d): (a) Adsorption isotherms of RhB by Gg-cl-P(AA-co-AAm)/Fe_3O_4 nanocomposite; (b) Langmuir isotherm; (c) Freundlich isotherm and (d) DKR isotherm for the adsorption of RhB by Gg-cl-P(AA-co-AAm)/Fe_3O_4 nanocomposite at different temperatures.

Langmuir isotherm model is best described by the following equation:

$$q_e = \frac{q_m \cdot b \cdot C_e}{1 + b \cdot C_e} \tag{6}$$

where, q_m is the maximum adsorption capacity (mg/g) of the adsorbent and b is the Langmuir constant related to the adsorption energy. The Langmuir isotherm equation can be rearranged to calculate Langmuir constants:

$$\frac{C_e}{q_e} = \frac{1}{q_m b} + \frac{C_e}{q_m} \tag{7}$$

The Langmuir constants can be calculated from the linear plot of C_e/q_e and C_e.

The applicability of Langmuir equation also depends upon the dimensionless factor R_L, which is given as:

$$R_L = \frac{1}{1 + b \cdot C_o} \tag{8}$$

where, C_o is the initial dye concentration (mg/L). Value of R_L between zero and one indicates the applicability of Langmuir adsorption isotherm. Value of R_L for all the three temperatures was found to be between zero and one which indicates the applicability of the Langmuir adsorption isotherm (Table 1).

DKR model is normally used to study the porosity of the adsorbent and apparent energy of the adsorption process. This model is represented by the following equation (Yan et al., 2012):

$$\ln\ q_e = \ln\ q_D - \beta \epsilon^2 \tag{9}$$

where, q_D is the mean adsorption capacity (mg/g), β is the activity coefficient and $\epsilon = RTln(1 + 1/C_e)$ and is called Polanyi potential. The values of q_D and β can be obtained from the intercept and slop of the plot between lnq_D and ϵ^2 and if the plot is a straight line then it proves the validity of this model but in this case the plot is not a straight line and the values of correlation coefficients for all the three temperatures is very poor which confirms the unapplicability of this model (Fig. 3(d)). The apparent energy of adsorption (E) can be obtained from the following equation:

$$E = \frac{1}{(2\beta)^{1/2}} \tag{10}$$

The experimental isotherm data was fitted to Eqs. (5), (7) and (9) by nonlinear regression and the results obtained are compiled in Table 1. The best fits were obtained with the Langmuir isotherm (Fig. 3(b)). The value of correlation coefficients for the three different temperatures i.e. 25, 35 and 45 °C were 0.999, 0.999 and 0.998, respectively which were much better than the values obtained from the fits of Freundlich isotherm (Fig. 3(c)) and DKR model (Fig. 3(d)). The value of mean adsorption capacity, q_D was found to be very less as compared to the values of Langmuir adsorption capacity at all the three temperatures. Difference in the values of

Table 1
Isotherm parameters for RhB adsorption onto Gg-cl-P(AA-co-AAm)/Fe_3O_4 nanocomposite.

Isotherms	Isotherm constants	Temperatures (°C)		
		25	35	45
Langmuir	q_m (mg/g)	529.10	584.79	654.87
	b (L/mg)	0.2160	0.1279	0.1224
	R^2	0.999	0.999	0.999
	R_L	0.007–0.033	0.012–0.054	0.013–0.057
Freundlich	$1/n$	0.2456	0.2989	0.3302
	K_F	174.26	148.48	146.02
	R^2	0.806	0.857	0.839
Dubinin–Kaganer–Radushkevich (DKR)	q_D (mg/g)	4.208	2.004	2.297
	E (KJ/mol)	12.50	18.25	17.14
	R^2	0.483	0.499	0.411

adsorption capacity by using these models may be due to the different assumptions taken into consideration during the formulations of these isotherm models. Value of maximum adsorption capacity was found to increase from 529.10 to 654.87 mg/g with the increase in temperature from 25 to 45 °C (Table 1).

The maximum adsorption efficiency of the nanocomposite for the adsorption of RhB obtained in this study was compared with other adsorbents reported in the literature (Table 2) and it was observed that the adsorption efficiency observed in this work is much better than the other adsorbents. Therefore, Gg-cl-P(AA-co-AAm)/Fe_3O_4 nanocomposite can be utilized for the successful adsorption of RhB from the dye contaminated water.

3.2.5. Thermodynamic parameters

Thermodynamic parameters were determined by using the Van't Hoff equation:

$$\ln\ K_L = \frac{\Delta S^\circ}{R} + \frac{-\Delta H^\circ}{RT} \tag{11}$$

$$\Delta G^\circ = -TT\ \ln\ K_L \tag{12}$$

$$K_L = m\frac{q_e}{C_e} \tag{13}$$

where, K_L is the distribution coefficient, ΔS° is the change in entropy, ΔH° is the change in enthalpy, ΔG° is the change in free energy, m is the adsorbent dose (g/L), q_e is the amount of the RhB adsorbed per unit mass of the adsorbent (mg/g), C_e is the equilibrium concentration (mg/L), T is the absolute temperature in K and R is the gas constant (8.314 JK^{-1} mol^{-1}). Values of ΔH° and ΔS° can be calculated from the slope and intercept of the linear plot of lnK_L and $1/T$ (Fig. S7, Supporting Information). The calculated values of change in enthalpy (ΔH°), change in entropy (ΔS°) and change in free energy (ΔG°) are given in Table 3. The positive value of ΔH° (27.71 kJ mol^{-1}) indicated the endothermic nature of the adsorption interactions and the positive value of ΔS° (17.00 kJ mol^{-1} K^{-1}) showed an increase in the disorder and randomness at solid–liquid interface (Bhaumik, Leswifi, Maity, Srinivasu, & Onyango, 2011; Khan, Dahiya, & Ali, 2012). The randomness at the solid-solution interface may be due to the more translational entropy gained by the displaced water molecules as compared to that lost by the dye molecules during the adsorption process (Gopal & Elango, 2007). The value of ΔG° was negative for all the three temperatures and was found to decrease from −14.07 at 25 °C to −15.01 kJ mol^{-1} at 35 °C. The feasibility of the spontaneous adsorption of RhB onto Gg-cl-P(AA-co-AAm)/Fe_3O_4 nanocomposites is favoured by the negative value of ΔG° (Ghorai, Sinhamahpatra, Sarkar, Panda, & Pal, 2012).

3.2.6. Adsorption kinetics

Effect of initial dye concentration of dye (50, 75 and 100 mg/L) and contact time on the adsorption of RhB is shown in Fig. 4(a). From the figure it is observed that the uptake of RhB molecules was very fast and increased with increase in time. It was also observed that the time required to reach equilibrium depends on the initial dye concentration. For the lowest dye concentration (50 mg/L), the adsorption equilibrium reached only in 30 min, for 75 mg/L the adsorption equilibrium reached in 90 min and for 100 mg/L the adsorption equilibrium reached in 240 min.

Pseudo first order, pseudo second order and intraparticle diffusion models were tested to examine the rate of the adsorption process and potential rate determining step.

Pseudo first order rate equation is:

$$\log\ (q_e - q_t) = \log\ q_e - \frac{k_1}{2.303}t \tag{14}$$

where, q_e (mg/g) is the equilibrium adsorption capacity, q_t (mg/g) is the adsorption capacity at time t and k_1 (1 min^{-1}) is the pseudo first order rate constant. Values of k_1 and q_e can be obtained from the slope and intercept of the plot of $\log(q_e - q_t)$ and t.

Table 2
Comparison of adsorption capacity of different adsorbents for the adsorption of RhB.

Adsorbent	q_m (mg/g)	Reference
Modifying Fe_3O_4 nanoparticles with humic acid	161.8	Peng et al. (2012)
Poly(glutamic acid)	390.2	Inbaraj, Chien, Hob, Yang, and Chen (2006)
Treated parthenium biomass	59.2	Lata, Mor, Garg and Gupt (2008)
Modified parthenium biomass	18.5	Lata, Garg, and Gupt (2008)
Kaolinite	46.08	Khan, Dahiya, and Ali (2012)
Jute stick powder	87.7	Panda, Das, and Guha (2009)
Scrap tires	280.1	Li, Liu, and Zhu (2010)
Bagasse pith	263.85	Gad and El-Sayed (2009)
Iron-pillared bentonite	98.62	Hou et al. (2011)
Duolite C-20 resin	28.57	Al-Rashed and Al-Gaid (2012)
Hypercross-linked polymeric adsorbent	2.1	Huang, Huang, Liu, Wang, and Yan (2008)
Gg-cl-P(AA-co-AAm)/Fe_3O_4 nanocomposite	654.87	This work

Table 3
Thermodynamic parameters for the adsorption of RhB onto Gg-cl-P(AA-co-AAm)/Fe_3O_4 nanocomposite.

ΔG° (kJ mol^{-1})			ΔH° (kJ mol^{-1})	ΔS° (kJ mol^{-1} K^{-1})
298.15 K	308.15 K	318.15 K		
−14.07	−14.54	−15.01	27.71	17.00

Pseudo second order rate equation is:

$$\frac{t}{q_t} = \frac{1}{k_2 q_e^2} + \frac{1}{q_e} t \quad (15)$$

where, k_2 (g/mg min) is the pseudo second order rate constant. The intercept and slope of the plot of t/q_t and t provides the values of k_2 and q_e.

The fitting to the experimental data using pseudo first order and pseudo second order is shown in Fig. 4(b–c), respectively. The values of correlation coefficients obtained from the pseudo second order (R^2 = 1.00–0.999) were much better than the values obtained from the pseudo first order (R^2 = 0.935–0.696), which showed that the experimental data of adsorption of RhB onto Gg-cl-P(AA-co-AAm)/Fe_3O_4 nanocomposite fitted better with pseudo second order rate equation than pseudo first order rate equation. Moreover, the value of k_2 was found to decrease with increased initial dye concentration which showed that the adsorption of RhB was faster for the lower concentrations. This may be due to the greater degree of distribution of dye over the surface of adsorbent for the adsorption process. Moreover, the calculated values of q_e by applying pseudo second order rate equation and the experimental values were almost same for all the concentrations studied, whereas q_e values obtained from pseudo first order rate equation showed a large deviation from the experimental values, which showed that the adsorption kinetics for the uptake of RhB by Gg-cl-P(AA-co-AAm)/Fe_3O_4 nanocomposite is best described by pseudo second order rate equation. The calculated values of correlation coefficients, adsorption capacities and rate constants are reported in Table 4.

Adsorption process includes various steps like passage of molecules of adsorbate from aqueous phase to the surface of adsorbent and the diffusion of adsorbate into the interior pores of the adsorbent. Intraparticle diffusion model determines the rate determining steps of the adsorption process and is best described by the intraparticle model given by Weber and Morris (1963):

$$q_t = k_i t^{0.5} + C \quad (16)$$

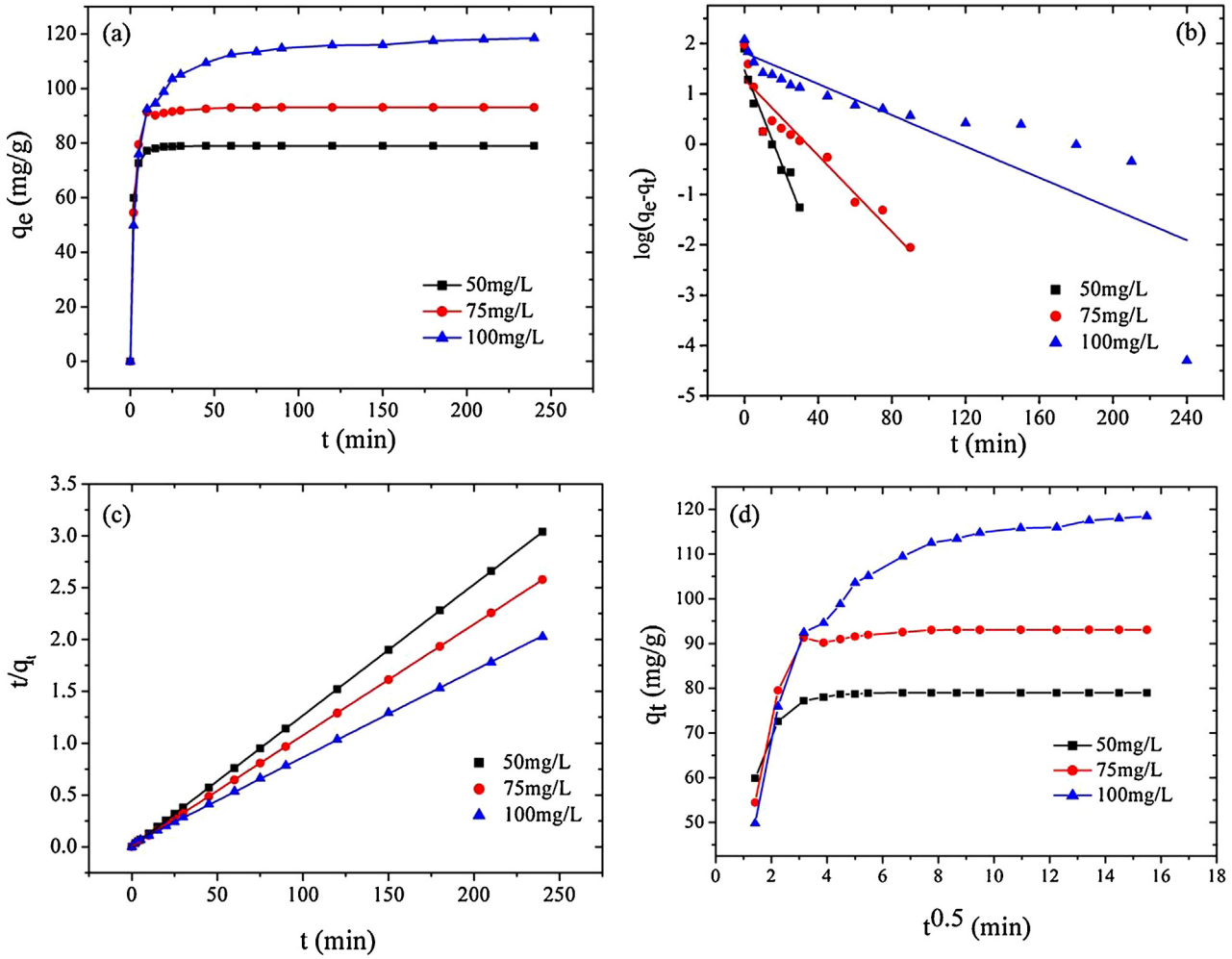

Fig. 4. (a) Kinetic data for the adsorption of RhB by Gg-cl-P(AA-co-AAm)/Fe_3O_4 nanocomposite; (b) fit of kinetic data to pseudo first order model; (c) fit of kinetic data to pseudo second order model and (d) fit of kinetic data to intraparticle diffusion model.

Table 4
Kinetic parameters for adsorption of RhB onto Gg-cl-P(AA-co-AAm)/Fe_3O_4 nanocomposite.

C_0 (mg/L)	q_e experimental (mg/g)	Pseudo first order			Pseudo second order			Intraparticle diffusion		
		k_1 (1 min^{-1})	q_e calculated (mg/g)	R^2	k_2 (g/mg min)	q_e calculated (mg/g)	R^2	k_i ($min^{0.5}$)	C	R^2
50	78.94	0.212	29.664	0.935	0.067	79.051	1.00	9.805	47.602	0.828
75	93.06	0.087	19.449	0.907	0.022	93.370	0.999	20.89	27.623	0.888
100	118.44	0.035	65.626	0.696	0.002	119.47	0.999	18.34	29.169	0.858

where, q_t (mg/g) is the adsorption capacity at time t and k_i (mg/g $min^{0.5}$) is the rate constant. The adsorption process is controlled by the intraparticle diffusion model if the plot of q_t vs. $t^{0.5}$ gives a straight line and passes through the origin. The plot of q_t vs. $t^{0.5}$ for different concentrations is shown in Fig. 4(d). From the figure it was observed that the plot of q_t vs. $t^{0.5}$ was not a straight line and did not pass through the origin, moreover, poor values of correlations coefficients i.e. 0.828, 0.888 and 0.858 were obtained for 50 mg/L, 75 mg/L and 100 mg/L, respectively (Table 4). This showed that the intraparticle diffusion was not the rate determining factor in the adsorption of RhB by Gg-cl-P(AA-co-AAm)/Fe_3O_4 nanocomposite.

3.2.7. Desorption studies

Higher adsorption capacity and high desorption efficiency are the characteristics of an advanced and efficient adsorbent. The reusability and reproducibility of an adsorbent reduces its overall cost. The desorption experiments of RhB from Gg-cl-P(AA-co-AAm)/Fe_3O_4 nanocomposite for the regeneration of active sites on adsorbent was conducted in 0.1 M HCl. Adsorbent was regenerated for five successive cycles and the adsorption and desorption of RhB were analyzed in each cycle of this experiment. Desorption kinetics of RhB from loaded Gg-cl-P(AA-co-AAm)/Fe_3O_4 nanocomposite and its performance for adsorption–desorption behaviour or the multiple cycles of regenerations is shown in Fig. S8, Supporting Information. Desorption equilibrium was attained in 60 min. Adsorption efficiency was found to remain constant for first three cycles however a slight decrease in the adsorption capacity (almost 12%) was observed in the last two cycles. Therefore, it is suggested from the desorption studies that Gg-cl-P(AA-co-AAm)/Fe_3O_4 nanocomposite can be repeatedly used as an efficient adsorbent for the removal of RhB from contaminated water.

3.2.8. Comparison of the adsorption efficiency of the nanocomposite with native polymer matrix

The comparison of the adsorption efficiency of the Gg-cl-P(AA-co-AAm)/Fe_3O_4 nanocomposite with native polymer i.e. Gg-cl-P(AA-co-AAm) for the adsorption of RhB was evaluated. The adsorption experiments were carried-out by adding optimum amount of the polymer (i.e. 0.6 mg/L) in the dye solutions of different concentrations varying in the range of 100–500 mg/L under similar experimental conditions as used for the adsorption of RhB using Gg-cl-P(AA-co-AAm)/Fe_3O_4 nanocomposite. The experimental data of the adsorption isotherm was fitted using Langmuir isotherm model and the maximum adsorption efficiency of 471.69 mg/g was observed, respectively (Table S2, Supporting Information). The adsorption efficiency of Gg-cl-P(AA-co-AAm) was found to be less than that of the nanocomposite. Higher adsorption efficiency of Gg-cl-P(AA-co-AAm)/Fe_3O_4 nanocomposite might be due to fact that the incorporation of MNPs within the polymer matrix increased the surface are and pore volume of the polymer as well as the number of the binding sites for the adsorption of dye also got increased by the incorporation of MNPs within the polymer matrix.

4. Conclusion

Fe_3O_4 MNPs have been successfully incorporated in the polymer matrix of Gum ghatti and acrylic acid-co-acrylamide based crosslinked polymers. BET, FT-IR, TEM, XRD and SEM evidenced the incorporation and uniform distribution of Fe_3O_4 MNPs within the polymer matrix. Gg-cl-P(AA-co-AAm)/Fe_3O_4 nanocomposite was very effective and efficient for the adsorption of RhB dye from contaminated water due to its high adsorption capacity, very rapid adsorption and working at pH 7; natural pH of most natural water resources. Adsorption of RhB dye onto Gg-cl-P(AA-co-AAm)/Fe_3O_4

nanocomposite was spontaneous, endothermic and accompanied with increase in entropy. The adsorption process followed the Langmuir adsorption model and the maximum adsorption capacity of 654.87 mg/g was observed. The adsorption process was better described by the pseudo second order kinetic model than other kinetic models with high correlation coefficients. The adsorbent showed very good reproducibility and reusability for the successive three cycles. Therefore, it is concluded that Gg-cl-P(AA-co-AAm)/Fe_3O_4 nanocomposite can be successfully utilized for the removal of rhodamine B from waste water.

Appendix A. Supplementary data

Supplementary data associated with this article can be found, in the online version, at http://dx.doi.org/10.1016/j.carbpol.2013.09.045.

References

Allegre, C., Maisseu, M., Charbit, F., & Moulina, P. (2004). Coagulation–flocculation–decantation of dye house effluents: Concentrated effluents. *Journal of Hazardous Materials*, *B116*, 57–64.

Al-Rashed, S. M., & Al-Gaid, A. A. (2012). Kinetic and thermodynamic studies on the adsorption behavior of rhodamine B dye on Duolite C-20 resin. *Journal of Saudi Chemical Society*, *16*, 209–215.

Badruddoza, A. Z. M., Tay, A. S. H., Tan, P. Y., Hidajat, K., & Uddin, M. S. (2011). Carboxymethyl-β-cyclodextrin conjugated magnetic nanoparticles as nano-adsorbents for removal of copper ions: Synthesis and adsorption studies. *Journal of Hazardous Materials*, *185*, 1177–1186.

Banerjee, S. S., & Chen, D. H. (2007). Fast removal of copper ions by gum Arabic modified magnetic nano-adsorbent. *Journal of Hazardous Materials*, *147*, 792–799.

Bhattacharyya, R., Ray, S. K., & Mandal, B. (2013). A systematic method of synthesizing composite superabsorbent hydrogels from crosslink copolymer for removal of textile dyes from water. *Journal of Industrial and Engineering Chemistry*, *19*, 1191–1203.

Bhaumik, M., Leswifi, T. Y., Maity, A., Srinivasu, V. V., & Onyango, M. S. (2011). Removal of fluoride from aqueous solution by polypyrrole/Fe_3O_4 magnetic nanocomposite. *Journal of Hazardous Materials*, *186*, 150–159.

Chang, Y. C., & Chen, D. H. (2005). Preparation and adsorption properties of monodisperse chitosan-bound Fe_3O_4 magnetic nanoparticles for removal of Cu(II) ions. *Journal of Colloid and Interface Science*, *283*, 446–451.

Crini, G. (2006). Non-conventional low-cost adsorbents for dye removal: A review. *Bioresource Technology*, *97*, 1061–1085.

Dogan, M., Alkan, M., & Onganer, Y. (2000). Adsorption of methylene blue from aqueous solution onto perlite. *Water, Air, and Soil Pollution*, *120*, 229–248.

Gad, H. M. H., & El-Sayed, A. A. (2009). Activated carbon from agricultural by-products for the removal of rhodamine B from aqueous solution. *Journal of Hazardous Materials*, *168*, 1070–1081.

Ghorai, S., Sinhamahpatra, A., Sarkar, A., Panda, A. B., & Pal, S. (2012). Novel biodegradable nanocomposite based on XG-g-PAM/SiO_2: Application of an efficient adsorbent for Pb^{2+} ions from aqueous solution. *Bioresource Technology*, *119*, 181–190.

Goncalves, I. M., Ferra, M. I., & Amorim, M. T. P. (1996). Processos de remocao biologica de corantes nos efluentes de industria textile. *Tecnologias do Ambiente*, *11*, 35–38.

Gopal, V., & Elango, P. (2007). Kinetic and thermodynamic investigations of adsorption of fluoride onto activated aloe vera carbon. *Journal of Indian Chemical Society*, *84*, 1114–1118.

Hao, O. J., Kim, H., & Chiang, P. C. (2000). Decolorization of wastewater. *Critical Reviews in Environmental Science and Technology*, *30*, 449–505.

Hou, M. F., Ma, C. X., Zhang, W. D., Tang, X. Y., Fan, Y. N., & Wan, H. F. (2011). Removal of rhodamine B using iron-pillared bentonite. *Journal of Hazardous Materials*, *186*, 1118–1123.

Huang, J. H., Huang, K. L., Liu, S. Q., Wang, T., & Yan, C. (2008). Adsorption of rhodamine B and methyl orange on a hypercrosslinked polymeric adsorbent in aqueous solution. *Colloids and Surfaces A: Physicochemical and Engineering Aspects*, *330*, 55–61.

Inbaraj, B. S., Chien, J. T., Hob, G. H., Yang, J., & Chen, B. H. (2006). Equilibrium and kinetic studies on sorption of basic dyes by a natural biopolymer poly (glutamic acid). *Biochemical Engineering Journal*, *31*, 204–215.

Kaith, B. S., Jindal, R., Mittal, H., & Kumar, K. (2012). Synthesis, characterization and swelling behavior evaluation of *Gum ghatti* and acrylamide based hydrogel for selective absorption of saline from different petroleum fraction-saline emulsions. *Journal of Applied Polymer Science*, *124*, 2037–2047.

Khan, T. A., Dahiya, S., & Ali, I. (2012). Use of kaolinite as adsorbent: Equilibrium, dynamics and thermodynamic studies on the adsorption of Rhodamine B from aqueous solution. *Applied Clay Science*, *69*, 58–66.

Kumari, K., & Abraham, T. E. (2007). Biosorption of anionic textile dyes by nonviable biomass of fungi and yeast. *Bioresource Technology*, *98*, 1704–1710.

Lata, H., Garg, V. K., & Gupt, R. K. (2008). Adsorptive removal of basic dye by chemically activated parthenium biomass: Equilibrium and kinetic modelling. *Desalination*, *219*, 250–261.

Lata, H., Mor, S., Garg, V. K., & Gupt, R. K. (2008). Removal of a dye from simulated waste water by adsorption using treated parthenium biomass. *Journal of Hazardous Materials*, *153*, 213–220.

Li, L., Liu, S., & Zhu, T. (2010). Application of activated carbon derived from scrap tires for adsorption of rhodamine B. *Journal of Environmental Sciences*, *22*, 1273–1280.

Lim, S. F., Zheng, Y. M., Zou, S. W., & Chen, J. P. (2009). Removal of copper by calcium alginate encapsulated magnetic sorbents. *Chemical Engineering Journal*, *152*, 509–513.

Mittal, H., Mishra, S. B., Mishra, A. K., Kaith, B. S., & Jindal, R. (2013). Flocculation characteristics and biodegradation studies of Gum ghatti based hydrogels. *International Journal of Biological Macromolecules*, *58*, 37–46.

Ncibi, M. C., Mahjoub, B., & Seffen, M. (2007). Kinetic and equilibrium studies of methylene blue biosorption by *Posidonia oceanica* (L.) fibres. *Journal of Hazardous Materials*, *B139*, 280–285.

Panda, G. C., Das, S. K., & Guha, A. K. (2009). Jute stick powder as a potential biomass for the removal of congo red and rhodamine B from their aqueous solution. *Journal of Hazardous Materials*, *164*, 374–379.

Papic, S., Koprivanac, N., Bozic, A. L., & Metes, A. (2004). Removal of some reactive dyes from synthetic wastewater by combined Al(III) coagulation/carbon adsorption process. *Dyes and Pigments*, *62*, 291–298.

Peng, L., Qin, P., Lei, M., Zeng, Q., Song, H., Yang, J., Shao, J., Liao, B., & Gu, J. (2012). Modifying Fe_3O_4 nanoparticles with humic acid for removal of Rhodamine B in water. *Journal of Hazardous Materials*, *209/210*, 193–198.

Rani, P., Sen, G., Mishra, S., & Jha, U. (2012). Microwave assisted synthesis of polyacrylamide grafted gum ghatti and its application as flocculant. *Carbohydrate Polymers*, *89*, 275–281.

Rocher, V., Siaugue, J. M., Cabuil, V., & Bee, A. (2008). Removal of organic dyes by magnetic alginate beads. *Water Research*, *42*, 1290–1298.

Sadeghi, S., Azhdari, H., Arabi, H., & Moghaddam, A. Z. (2012). Surface modified magnetic Fe_3O_4 nanoparticles as a selective sorbent for solid phase extraction of uranyl ions from water samples. *Journal of Hazardous Materials*, *215/216*, 208–216.

Sand, A., Yadav, M., & Behari, K. (2010). Graft co-polymerization of 2-acrylamidoglycolic acid onto xanthan gum and study of its physicochemical properties. *Carbohydrate Polymers*, *81*, 626–632.

Singh, V., Kumari, P., Pandey, S., & Narayan, T. (2009). Removal of chromium (VI) using poly(methylacrylate) functionalized guar gum. *Bioresource Technology*, *100*, 1977–1982.

Singh, V., Tiwari, S., Sharma, A. K., & Sanghi, R. (2007). Removal of lead from aqueous solutions using Cassia grandis seed gum-graft-poly(methylmethacrylate). *Journal of Colloid and Interface Science*, *316*, 224–232.

Waranusantigul, P., Pokethitiyook, P., Kruatrachue, M., & Upatham, E. S. (2003). Kinetics of basic dye (methylene blue) biosorption by giant duckweed (*Spirodela polyrrhiza*). *Environmental Pollution*, *125*, 385–392.

Weber, W. J., Jr., & Morris, J. C. (1963). Kinetics of adsorption on carbon from solution. *Journal of Sanitary Engineering Division: American Society of Civil Engineers*, *89*, 31–59.

Xu, Y. Y., Zhou, M., Geng, H. J., Hao, J. J., Ou, Q. Q., Qi, S. D., et al. (2012). A simplified method for synthesis of Fe_3O_4@PAA nanoparticles and its application for the removal of basic dyes. *Applied Surface Science*, *258*, 3897–3902.

Yan, H., Yang, L., Yang, Z., Yang, H., Li, A., & Cheng, R. (2012). Preparation of chitosan/poly(acrylic acid) magnetic composite microspheres and applications in the removal of copper(II) ions from aqueous solutions. *Journal of Hazardous Materials*, *229/230*, 371–380.

Zhou, Y. T., Nie, H. L., Branford-White, C., He, Z. Y., & Zhu, L. M. (2009). Removal of Cu^{2+} from aqueous solution by chitosan-coated magnetic nanoparticles modified with α-ketoglutaric acid. *Journal of Colloid and Interface Science*, *330*, 29–37.